Electrostatic complementarity in an aldose reductase complex from ultra-high-resolution crystallography and first-principles calculations

Nicolas Muzet, Benoît Guillot, Christian Jelsch, Eduardo Howard, Claude Lecomte

PNAS 2003 July, 100 (15) 8742-8747.

https://doi.org/10.1073/pnas.1432955100

Communicated by Herbert Hauptman, Hauptman–Woodward Medical Research Institute, Buffalo, NY,

May 16, 2003 (received for review October 30, 2002)

Electrostatic complementarity in an aldose reductase complex from ultra-high-resolution crystallography and first-principles calculations

Nicolas Muzet*, Benoit Guillot*, Christian Jelsch*, Eduardo Howard†‡, and Claude Lecomte*§

*Laboratoire de Cristallographie et Modélisation des Maté´ riaux Minéraux et Biologiques, Centre National de la Recherche Scientifique Unité Mixte de Recherche 7036, Université Henri Poincaré , Faculté des Sciences, BP 239, 54506 Vandoeuvre-le` s-Nancy, France; and †Department of Structural Biology, Institut de Génétique et de Biologie Moléculaire et Cellulaire, 1 Rue Laurent Fries, 67404 Illkirch, France

Classification: Biological Sciences: Biophysics. Computational chemistry. Crystallography

ABSTRACT

The electron density and electrostatic potential in an Aldose Reductase holoenzyme complex have been studied by DFT and diffraction methods. Aldose reductase is involved in the reduction of glucose in the polyol pathway using NADPH as a co-factor. The ultra-high resolution of the diffraction data and the low thermal displacement parameters of the structure allow accurate atomic positions and an experimental charge density analysis. Based on the X-ray structural data, order-*N* Density Functional Theory (DFT) calculations have been performed on 711 atoms in the active site of the molecule. The charge density refinement of the protein was performed with program MoPro using the transferability principle and our database of charge density parameters built from crystallographic analyses of peptides and amino acids.

Electrostatic potentials calculated from the charge density database, from the preliminary experimental electron density analysis, from DFT computations, and from atomic charges taken from the AMBER software dictionary are compared. The electrostatic complementarity between the co-factor $NADP^+$ and the active site shows up clearly. The anchoring of the inhibitor is due mainly to hydrophobic forces and to only two polar interaction sites within the enzyme cavity. The potentials calculated by X-Ray and DFT techniques agree reasonably well. At the present stage of the refinement, the potentials obtained directly from the database are in excellent agreement with the experimental ones, as well as with the DFT ones. These results demonstrate in addition the significant contribution of atomic polarization effects to the host and guest mechanism.

INTRODUCTION

We have recently shown that accurate electron density analyses may be carried out on proteins if ultra-high resolution data are available[1]. Experimental charge density methods[2-4] give an analytical representation of the valence electron density[5] from the refinement of aspherical atomic scattering factors (program MoPro)[6]. Starting electron density parameters may be obtained from our oligopeptide charge density database[7]. Therefore, any property depending on the static charge density may be computed[8]: one of the properties of greatest importance for drug design and biochemistry in general is the electrostatic potential which provides information about reactivity[9]. Correspondingly, order-*N* DFT methods may be used for estimating precisely the valence charge density and the related properties of proteins and large molecules[10,11].

Podjarny and collaborators[12,13] have recently collected accurate diffraction intensities to ultra-high resolution (0.66 Å) on an enzymatic complex: aldose reductase (AR) + $NADP^+$ cofactor + inhibitor IDD 594 (Fig. 1). This system gives a unique opportunity to test the accuracy of theoretical methods for calculating the electrostatic potential in protein complexes compared to experiment and vice versa. Therefore, we report on the crystallographic and DFT electrostatic properties of the aldose reductase

complex, a 315 amino-acid protein involved in diabetic complications, studied largely for the purpose of inhibitor development.

Aldose reductase is involved in the first step of the sorbitol pathway: glucose is reduced to sorbitol by aldose reductase with NADPH as a cofactor. When there is an abnormal glucose excess in tissues, the accumulation of sorbitol leads to biochemical alterations which can result in lesions[14]. This study contributes to the search for inhibitors for the pharmacotherapy of diabetic complications through the analysis of electrostatic forces in the cofactor and inhibitor binding. For the first time, the host-guest mechanism is analysed at a detailed level that goes beyond usual structural and steric features. The contribution of atomic polarization effects on the electrostatic complementarity of the protein active site with its ligands will be demonstrated by ultra-high resolution crystallography and order-*N* DFT methods.

MATERIALS AND METHODS

The crystallization of aldose reductase was described by Podjarny and coll.[12]. The crystals are monoclinic of space group $P2_1$ (a=49.43, b=66.79, c=47.40Å, β=92.40° and one molecule per asymmetric unit). The 0.66Å resolution diffraction data of the aldose reductase - $NADP^+$ - IDD 594 complex (Fig. 1) were collected at a temperature of 100K on the ID19 beamline at the Advanced Photon Source (Argonne, USA)[13]. A total of 2 262 072 reflections have been measured from two crystals and were merged with program SCALEPACK[15] to 511 265 unique reflections ($R_{int}(I)$=2.9% and 2.7% for crystals 1 and 2). 80% of the merged reflections have their intensities larger than 3.sigma. The completeness of the data is 89% ($0.66 < d < 20$ Å) The structure was first determined by Cachau *et al.*[13] using the SHELXL-97 program[16]. The refined protein structure model includes all the (non-water) hydrogen atoms and 629 water molecules.

The charge density refinement strategy with program MoPro[6] was the following. Starting position and thermal parameters were those of Cachau *et al.*[13] and the initial charge density parameters were those of neutral spherical atoms. As the thermal motion in some parts of the protein (especially in the N- and

C-terminal parts) does not allow a charge density analysis, a subset of the structure was selected, based on atomic equivalent thermal *B* factors lower than about 8 $Å^2$. This charge-density-refinement substructure included all main chain-atoms, except the three N- and three C-terminal amino acids and the Trp219-Ser226, Glu229-Asp230 and Phe276-Val297 residue ranges.

At first, a high-order spherical atom refinement was performed with the program MoPro[6] on the non-hydrogen atoms of the substructure, in order to start the electron density refinement with the least biased positional and thermal parameters. This refinement was performed against high-resolution shells of decreasing size. The three successive resolution ranges used were 0.5-0.76 $Å^{-1}$ (327 546 reflections), 0.6-0.76 $Å^{-1}$ (216 984) and 0.65-0.76 $Å^{-1}$ (152 454). A zero intensity over sigma cutoff, which corresponds to a completeness of 68% for the highest resolution shell (0.7-0.76 $Å^{-1}$), was applied. The high-order refinement strategy consisted of alternate refinement of positional and anisotropic thermal motion parameters, without any stereochemical or dynamical restraints, until total convergence, for each of the three resolution ranges. In each case, significant improvements in the agreement factors $R(F)$ and $R_{free}(F)$ were observed. For example, in the 0.65-0.76 $Å^{-1}$ range, the $R(F)$ factor dropped from 13.79% to 13.41%.

In the second stage of refinement, the starting electron density parameters were transferred from our aspherical atoms multipole database[7] describing all the chemical groups present in proteins. All atoms of the protein were assigned non-spherical scattering factors; water molecules were modelled as free oxygen atoms. The starting parameters for $NADP^+$ were from the charge density analysis of NAD^+[11], and spherical atom scattering factors were used for the IDD 594 inhibitor compound. All hydrogen atoms were displaced along the X-H bonds to standard bond distances obtained by neutron diffraction studies[17] and were subsequently kept fixed.

The transfer procedure leads to an immediate improvement of statistical agreement indices, with the $R(F)$ factor dropping from 11.45 to 11.05% and the $R_{free}(F)$ from 12.07 to 11.77% for 467 214 reflections with $I/\sigma_I > 0$ and $0<d<0.66Å$. This decrease of the crystallographic *R*-factors, and the improvement of the resulting residual density, fully justify the multipolar parameters transfer procedure.

The electron density refinement was performed with MoPro for the main chain atoms (including hydrogen atoms) of the substructure described above, against the 456 477 reflections in the 0.15-0.76 $Å^{-1}$ resolution range. For the atoms of the protein side chains, of the ligands and of the water molecules, only positions and thermal parameters were refined. This charge density analysis included the refinement of the multipolar parameters and the valence populations. Electron density constraints were applied taking advantage of the essential chemical equivalence of the peptide units. Local symmetry constraints were also applied as only the non-zero multipole parameters of the databank were allowed to vary.

The low resolution truncation makes some allowance for the problem of the disordered solvent, as an exponential scaling model turned out not to be helpful at this stage of our study. One of the next improvement of the procedure will be to perform the bulk solvent correction, using the flat solvent model[18].

This preliminary charge density refinement lead to a description of the average electron density and atomic charges along the main chain, which was subsequently used for a computation of the electrostatic potential. The resulting set of valence population parameters (P_v) for the protein main-chain atoms are Cα 4.04(7), O: 6.32(8), N: 5.12(7), C: 4.09(7), Hα: 0.86(9) and H_N: 0.81(8) (*R(F)* factor drops from 10.21% to 10.10% and $R_{free}(F)$ from 11.04% to 10.68% in the 0.15-0.76$Å^{-1}$ resolution range). The experimental charge density refinement of the aldose reductase complex is still being completed and will be reported in detail in a forthcoming paper.

DFT calculations

All calculations were performed at the experimental geometry with the DFT code SIESTA[19,20]. This software allows calculations that scale linearly with, rather than with the cube of the number of atoms in the system. This allowed the study of large parts of the aldose reductase complex. Some of the approximations made are described in the following, and a detailed description could be found in references[19-21].

Exchange and correlation of the Kohn-Sham theory[22] are treated with the Generalized Gradient Approximation (GGA) functional proposed by Perdew, Burke, and Ernzerhof (PBE)[23]. Core electrons were replaced by scalar-relativistic norm-conserving pseudopotentials generated using the Troullier-Martins schem[24] in their fully non-local formulation[25]. A uniform mesh with a plane-wave cut-off of 75 Ry was used to represent the Hartree and exchange-correlation potentials and the local part of the pseudopotential.

Valence electrons were described using a basis set of finite-range numerical atomic orbitals. Radial parts of these orbitals are based on the scheme of pseudo-atomic orbitals of Sankey and Niklewski[26] who proposed a scheme to build single-ζ bases. In SIESTA, the bases are generalized to arbitrarily complete bases up to double-ζ with polarization orbitals[21]. The orbital confinement energies used have been defined in an earlier report[10], where the final set of cutoff values were selected so the electronic density would be comparable to the experimental density in the database. Use of these finite range orbitals, which give rise to sparse overlap and Hamiltonian matrices, and of pseudo potentials in the Kleinman-Bylander factorized form, allows the Kohn-Sham Hamiltonian to be built with order-N operations. More details on these techniques are given in references[19-21].

The DFT quantum chemical modeling included:

- a 603 atom substructure consisting of 64 amino acid residues that surround the active site
- a 676 atom substructure consisting of the 64 active site residues plus, the NADP+ cofactor
- a 703 atom substructure including additionally the IDD594 inhibitor

For these calculations, the atomic positions were held fixed at the crystallographic geometry.

were carried out on 64 active-site amino acids, the cofactor and the inhibitor for the holoenzyme (711 atoms), and then on the same amino acids (603 atoms) for the active site alone. A third calculation was performed on the active site and the cofactor, but without the inhibitor (676 atoms). The 64 amino acids in the DFT-calculation substructure completely surround the cofactor $NADP^+$ nicotinamide moiety and the inhibitor.

Electrostatic potential

The experimental electrostatic potentials were computed from the electron density at the refined geometry with program ELECTROS[27] in two ways: first (TRF), using directly the charge density parameters transferred from the aspherical-atom, multipole database[7,28]; and, second (MUL), using the parameters obtained from the preliminary multipole refinement of the protein main-chain atoms. The experimental potential of $NADP^+$ was derived from the NAD^+ charge density analysis reported previously[11].

The theoretical DFT potential was obtained from the SIESTA calculations. For the analysis of the binding interactions, the electrostatic potential of the cofactor $NADP^+$, of the inhibitor, and of the enzyme active site were computed separately "*in vacuo"* without any interaction and compared to the electrostatic potential generated by the complex. The electrostatic potential (AMB) generated by the protein without the cofactor was computed using the force field charges of the AMBER dictionary[29].
For both methods, the electrostatic potential was computed using the 64 amino acids substructure surrounding the active site (603 atoms), plus the $NADP^+$ cofactor and inhibitor atoms leading to a total of 711 atoms.

RESULTS

Quality of the TRF electrostatic potential

The electrostatic potential generated by the NADP+ cofactor is shown in Fig. 3. The DFT and TRF potential compare well around the nicotinamide moiety, while the negative potential around the pyrophosphate group of $NADP^+$ appears significantly stronger in the DFT map than in the theoretical map.

The potential in the protein active site obtained by DFT can be compared to the transferred experimental TRF potential obtained directly from the charge density database in Figures 4ab, 5bc and 6bd. The agreement between the DFT and TRF maps is generally good: the positive and negative potential regions are similar; the TRF negative potential well being generally deeper.

The good agreement demonstrates that a TRF electrostatic potential calculated – at small computing cost – using the database of charge and multipole parameters[7] and high resolution (d < 1.5 Å) crystallographic atomic positions (including hydrogen atoms) is very reliable, and can be obtained routinely as soon as a high-resolution structure with hydrogen atoms is available.

Electrostatic complementarity of ligand–protein interactions.

$NADP^+$ is naturally bound by aldose reductase to enable sugar hydroxyl reduction. Although, in the crystal studied, the ligand is not a sugar but an inhibitor, it is likely that $NADP^+$ interacts in a very similar way with the protein. The cofactor is made of five functional groups, namely, nicotinamide, ribose, pyrophosphate, ribose, and adenine. In the studied complex, the first three groups are buried within the active site, whereas the last two are partly outside of the protein, solvated by water molecules.

The $NADP^+$ cofactor alone displays a large negative potential around the pyrophosphate group (DFT: –0.28 e/Å, TRF: –0.40 e/Å) near the pyrophosphate oxygen atoms, and a positive potential around the nicotinamide ring due to the global positive charge of the protonated base (Figure not shown). The oxygen of the $NADP^+$ amide group generates a small negative potential (DFT: -0.04 e/Å, TRF: -0.04 e/$Å^3$). The zero level contour is very similar for the two methods. Fig. 4 shows the electrostatic potential in the nicotinamide ring plane generated by the apoenzyme alone calculated by the MUL, TRF, and DFT methods and from the AMBER point charges (AMB). As discussed previously MUL and TRF potentials are in good agreement .

By comparison with **Erreur ! Source du renvoi introuvable.**3, both DFT and TRF (MUL) apoenzyme electrostatic potentials clearly display genuine complementarity with the $NADP^+$ potential. To each negative potential region around the cofactor (pyrophosphate group and amide oxygen atom) corresponds a positive potential region in the active site: the enzyme positive regions are located near Pro211 and Ser210 (Fig. 4) (DFT: +0.34, TRF: +0.18, MUL: +0.14, AMB: +0.14 e/Å) and near Asn160-NH_2 and His110 $N^{\varepsilon 2}$–$H^{\varepsilon 2}$ (DFT: +0.20, TRF: +0.26, MUL: +0.12, AMB: +0.06 e/Å).

Fig. 4 also reveals two negative potential wells: one close to Cys298 S^{γ} (DFT: -0.18 e/Å, TRF: - 0.06 e/Å, MUL: -0.08 e/Å, AMB: -0.04 e/Å) and the second one near Asp43-$O^{\delta 1}$ (DFT: -0.28 e/Å, TRF: -0.14 e/Å, MUL: -0.14 e/Å, AMB: -0.18 e/Å). In the enzyme-cofactor interaction, these two negative potential regions complement the strong positive potential of $NADP^{+}$. The second of the two negative potential wells is created by a special configuration of at least ten protein atoms: one sulfur (Cys298 S^{γ}) and nine oxygen atoms (Cys298 O, Tyr209 OH, Gln183 $O^{\varepsilon 1}$ and O, Asp43 $O^{\delta 1}$, $O^{\delta 2}$ and O, and Thr19 O and $O^{\gamma 1}$) all of which are nearly located in a plane almost perpendicular to the nicotinamide ring. An important point is that most of these atoms do not interact directly with $NADP^{+}$. Only three of them form hydrogen bonds with $NADP^{+}$: Cys298 S^{γ}, Asp43 $O^{\delta 1}$, and Gln183 O (Fig. 2 & Table 1). It is clear that all other atoms contribute through long-range electrostatic attraction to the binding of the cofactor. These results demonstrate that considering only the short-range H-bonds involved in the ligand binding clearly underestimates the interaction strength.

Although, there is a qualitative agreement among the four techniques of potential computation, some differences remain. A significant one is that the AMBER charges yield a weaker negative potential near Cys298 S^{γ} . Also, all the positive AMB potentials seem to be lower than the DFT, TRF, and MUL values. The similarity of the DFT, TRF, and MUL potentials indicates that they are more precise than point-charge point potentials, apparently because they take into account a certain degree of atomic polarization. Further crystallographic refinement of the side chains, including Cys298 S^{γ} , will further clarify this point.

Inhibitor - active site interactions

The chemical structure of the *IDD594* inhibitor (Figure 1) differs significantly from that of glucose, but the inhibitor carboxylate group should bind in a similar region of the enzyme active site as the reacting hydroxyl group of glucose[13,14]. As no high resolution data exists for the glucose complex, the discussion will focus on inhibitor interactions. The charge density refinement of the inhibitor was done *ab initio*, due to the lack of multipole values in the database for the specific chemical groups. Therefore the IDD594 electrostatic potentials displayed in the present study are derived from the DFT

calculations only. Fig. 5 gives the DFT potential generated by the inhibitor. Except for the carboxylate group, the potential is slightly positive without any large extension, reflecting the hydrophobic nature of the compound. An orthogonal view (not shown) gives similar information, except a slightly negative well (DFT value: -0.02 e/Å) in the vicinity of the Br-bearing aromatic ring leading to a π-π interaction with Trp111. This contrasts with the binding of $NADP^+$ which is strongly electrostatic. Fig. 5 also shows that the corresponding cavity of the apoenzyme displays an overall low positive potential with two negative wells created by Cys80 S^{γ} and the Thr113 hydroxyl group (DFT: -0.1 e/Å, TRF: -0.2 e/Å, MUL: -0.25 e/Å). The experimental MUL and TRF maps gave a stronger negative potential around Tyr309 (TRF & MUL : -0.10 e/Å) whereas the theoretical value is slightly positive (DFT: +0.02 e/Å).

The bromine atom of the inhibitor forms an exceptionally short contact with the $O^{\gamma 1}$ oxygen atom of Thr113 (distance = 3.0 Å). This is the shortest Br…O contact observed so far according to the Cambridge Structural Database[30]. Fig. 6 shows the potential around the bromine atom, within the protein complex, for the ligand alone and for the active site. The hydroxyl hydrogen atom of the Thr113 is not directed towards the bromine atom, as might have been expected, but is involved instead in a hydrogen bond with the Thr113 carbonyl. The negative potential due to the lone pairs of $O^{\gamma 1}$ of Thr113 can be directly superposed with the positive potential developed by the bromine atom of the inhibitor; this renders this short interaction essentially electrostatic. The theoretical deformation density maps also reveals effects of the interaction on the bromine (Fig. 7a , shown in the same plane as Fig. 6). The orthogonal views of the torus-shaped deformation density around the Br atom (Fig. 7b and c), for the ligand alone and in the complex, reveal the effects of the interaction on the bromine atom. Through the interaction with the $O^{\gamma 1}$ of Thr113, the bromine atom is polarized and looses its cylindrical symmetry.

The second polar interaction site of the ligand is located on the other side of the molecule (Fig 1). The carboxylate group interacts strongly with the enzyme by the means of two hydrogen bonds (Table 1). Fig. 8a, 8b and 8c display respectively the DFT potential generated in the carboxylate plane by the

ligand alone, by the apoenzyme active site and by the complex. Fig. 8d represents the TRF electrostatic potential equivalent to the DFT one drawn Fig. 8b. The DFT electrostatic potentials in the plane perpendicular to the inhibitor carboxylate are represented around the ligand alone (Fig. 9a), in the active site of the protein alone (Fig. 9b) and in the active site of the protein – $NADP^+$ complex (9c) with its TRF counterpart (9d). Both Figs. 8 and 9 show the excellent agreement between experimental and theoretical active site potentials, which confirms the feasibility of interactions analyses using the database and high resolution X-rays refinement only. There is a local complementarity between the potentials; in addition, several electrostatic potential saddle points, characteristic of H-bonds, can be observed. The potential in the plane perpendicular to the inhibitor carboxylate (Fig. 9) shows that the attraction of the ligand carboxylate requires the presence of the $NADP^+$ cofactor. The positively charged nicotinamide group contributes to the electrostatic complementarity and therefore to the anchoring of the inhibitor carboxylate (Fig. 9c,d). Indeed, without the cofactor (Fig. 9a), the protein active site displays a large negative potential that would hinder the binding of COO^- (Fig. 9b).

DISCUSSION AND CONCLUSION.

Obtaining accurate electrostatic properties to understand interactions among proteins, ligands, and cofactors is very challenging and has many potential applications in life sciences as shown by the increasing number of publications devoted to this topic. First, this research needs atomic resolution diffraction data in order to be able to locate and refine the hydrogen atoms of the active site. The use of dipolar scattering factors for hydrogen atoms, as defined in our database, is necessary. Recent developments of diffraction techniques at third generation synchrotrons[31] and progress in cryocrystallography[32] and protein crystallization promise more and more high resolution data, which will deserve aspherical atom models to yield more accurate atomic coordinates and thermal displacement parameters. This will also permit more precise location of molecules and ions with important roles in bioelectrostatics in the protein solvation shell. Given a well refined high-resolution structure, electrostatic properties may be calculated in different ways: either directly by multipolar analysis or using DFT (this work) and/or QM/MM methods[33-35]; fragments experimentally (TRF[27], this

work) or theoretically calculated[36-40]; or computationally by point charge models such as AMBER[29] , CHARMM[41] or GRASP[42].

This paper has demonstrated that DFT quality potentials can be obtained quickly and almost routinely from high-resolution diffraction data (TRF Potentials). More generally, such a calculation can be routinely performed, at very low cost, to any protein structure at atomic resolution. A direct experimental determination from an accurate experimental charge density distribution is also possible, as shown in this paper (MUL). But this latter possibility still needs further testing and development tests to define the best refinement strategies (even though the refinement program MoPro is available) to ensure that the resulting potential is more accurate than the database-transferred one. This issue will be discussed in a forthcoming publication.

Concerning the complex aldose reductase – $NADP^+$ – inhibitor , and enzymology more generally, this work reports, for the first time to our best knowledge, an experimental and theoretical analysis of the protein host-guest interaction at the electrostatic level, i.e. beyond geometrical or putative hydrogen bonding considerations. The role of Coulombic long-range interactions and of atomic polarizability have also been clearly evidenced in the aldose reductase-cofactor complex. The results has remarkably good electrostatic apoenzyme-cofactor complementarity within the active site, and good hydrophilic/hydrophobic complementarity between the enzyme and the inhibitor. The carboxylate group of the inhibitor is the source of the main polar interaction with the enzyme, and the electrostatic complementarity is with the positive potential produced by the $NADP^+$ cofactor. In addition, the polarizable bromine atom of the inhibitor forms a short polar contact with an hydroxyl oxygen atom.

Further work is planned with aldose reductase to develop optimal charge density refinement and potential mapping strategies, and to evaluate apoenzyme-cofactor-ligand electrostatic interaction energies.

Acknowledgements. We gratefully acknowledge Alberto Podjarny and collaborators for providing us with the aldose reductase data and Pr. Emilio Artacho and Maria Victoria Fernandez-Serra for helpful discussions on the SIESTA program. Our colleague, V. Pichon-Pesme, is greatly acknowledged for the many discussions about the database. NM was supported by a grant of the Association pour la Recherche sur le Cancer and BG by a fellowship of the French Minister of Research and Technology.

References

(1) Jelsch, C., Teeter, M. M., Lamzin, V., Pichon-Pesme, V., Blessing, R. H. & Lecomte, C. (2000) *Proc. Natl. Acad. Sci. USA.* **97**, 3171-3176.

(2) Lecomte, C. (1995) *Adv. Molecular Structure Res.* **1**, 261-302.

(3) Coppens, P. (1998) *Acta Cryst. A* **54**, 779-788.

(4) Coppens, P. (1997) *X-ray charge densities and chemical bonding. IUCR*. Ed. Oxford University Press.

(5) Hansen, N. K. & Coppens, P. (1978) *Acta Cryst. A* **34**, 909-921.

(6) Guillot, B., Viry, L., Guillot, R., Lecomte, C. & Jelsch, C. (2001). *J. Appl. Cryst*. **34**, 214-223.

(7) Pichon-Pesme, V., Lecomte, C. & Lachekar, H. (1995) *J. Phys. Chem.* **99**, 6242-6250.

(8) Stewart, R. F. (1976) *Acta Cryst. A* **32**, 565-574.

(9) Politzer, P. & Murray, J. S. (1993) *Trans. Am. Cryst. Ass.* **26**, 23-40.

(10) Fernandez-Serra, M. V., Junquera, J., Jelsch, C., Lecomte, C. & Artacho, E. (2000) *Solid State Comm.* **116**, 395-400.

(11) Guillot, B., Muzet, N., Jelsch, C., Artacho, E. & Lecomte, C. (2002) *submitted*.

(12) Lamour, V., Barth, P., Rogniaux, H., Poterszman, A., Howard, E., Mitschler, A., Van Dorsselaer, A., Podjarny, A. & Moras, D. (1999) *Acta Cryst. D* **55**, 721-723.

(13) Cachau, R., Howard, E., Barth, P., Mitschler, A., Chevrier, B., Lamour, V., Joachimiak, A., Sanishvili, R., Van Zandt, M., Sibley, E., Moras, D. & Podjarny, A. (2000) *Journal de Physique* **10**, 3-13.

(14) Yabe-Nishimura, C. (1998) *Pharmacological review* **50(1)**, 21-32.

(15) Otwinowski, Z & Minor, W. (1997) *Methods in Enzymology* **276**, 307-326.

(16) Sheldrick, G. M. (1997) *SHELXL97 Program for the Refinement of Crystal Structures* Sheldrick, G. M., Ed.: University of Göttingen, Germany.

(17) Allen, F. (1986) *Acta Cryst. B* **42**, 515-522.

(18) Jiang, J.-S. & Brünger, A. T. (1994) *J. Mol. Biol.* **243**, 100-115.

(19) Sanchez-Portal, D., Ordejon, P., Artacho, E. & Soler, J. M. (1997) *Int. J. Quant. Chem.* **65**, 453-461.

(20) Soler, J. M., Artacho, E., Gale, J. D., Garcia, A., Junquera, J., Ordejon, P. & Sanchez-Portal, D. (2002) *J. Phys. Condens. Matt.* **14**, 2745-2779.

(21) Artacho, E., Sanchez-Portal, D., Ordejon, P., Garcia, E. & Soler, J. M. (1999) *Phys. Stat. Sol. B* **215**, 809-817.

(22) Kohn, W. & Sham, L. J. (1965) *Phys. Rev.* **140**, 1133-1136.

(23) Perdew, J. P., Burke, K. & Ernzerhof, M. (1996) *Phys. Rev. Lett.* **77**, 3865-3868.

(24) Troullier, N. & Martins, J.-L. (1991) *Phys. Rev. B* **43**, 1993-2006.

(25) Kleinman, L. & Bylander, D. M. (1982) *Phys. Rev. Lett.* **48**, 1425-1428.

(26) Sankey, O. F. & Niklewski, D. J. (1989) *Phys. Rev. B* **40**, 3979-3995.

(27) Bouhmaida, N., Ghermani, N.-E., Lecomte, C. & Thallal, A.(1999) *Acta Cryst. A* **55**, 729-738.

(28) Jelsch, C., Pichon-Pesme, V., Lecomte, C. & Aubry, A. (1998) *Acta Cryst. D* **54**, 1306-1318.

(29) Bayly, C. I., Cieplak, P., Cornell, W. D. & Kollman, P. A. (1993) *J. Phys. Chem.* **97**, 10269-10280.

(30) Allen, F. H. & Kennard, O. (1983) *Chem. Design Automation News* **8**, 31-37.

(31) Longhi, S., Czjzek, M. & Cambillau, C. (1998) *Curr. Opin. Struct. Biol.* **8**, 730-737.

(32) Samygina, V. R., Antonyuk, S. V., Lamzin, V. S. & Popov, A. N. (2000) *Acta Cryst. D* **56**, 595-603.

(33) Eurenius, K. P., Chatfield, D. C., Brooks, B. R. & Hodoscek, M. (1996**)** *Int. J. Quant. Chem.* **60(6)**, 1189-2000.
(34) Gao, J. (1996) *Acc. Chem. Res.* **29**, 298-305.
(35) Leach, A. R. (1996) *Molecular Modelling Principles and Applications*; Longman ed, Essex.
(36) Karle, J., Huang, L. & Massa, L. (1998) *Pure & Appl. Chem.* **70**, 319-324.
(37) Walker, P. D. & Mezey, P. G. (1994) *J. Am. Chem. Soc.* **116**, 12022-12032.
(38) Bader, R. W. F. (1990) *Atoms in Molecules. A Quantum Theory*; Oxford Science Publications: Oxford.
(39) Koritsanszky, T., Volkov, A. & Coppens, P. (2002) *Acta Cryst. A* **58**, 464-472.
(40) Dittrich, B., Koritsánszky, T., Grosche, M., Scherer, W., Flaig, R., Wagner, A., Krane, H. G., Kessler, H., Riemer, C., Schreurs, A. M. M. & Luger, P. (2002) *Acta Cryst. B* **58**, 721-727.
(41) Brooks, B. R., Bruccoleri, R. E., Olafson, B. D., States, D. J., Swaminathan, S. & Karplus, M. (1983) *J. Comp. Chem.* **4**, 187-217.
(42) Honig, B. & Nicholls, A. (1995). *Science* **268**, 1144-1149.

Table 1. Distances and angles of the hydrogen bonds involving $NADP^+$ or the inhibitor.

Acc…Donor	AD	DHA
IDD594-IDD594	(Å)	(°)
O34...N17	2.98()	174()
$NADP^+$–protein		
O15...N_T19	3.25	152
O16...N_W20	2.90	137
O11...N^{ζ}_K21	2.82	150
O17...$N^{\delta 2}$_N160	2.89	165
O12...O^{γ}_S210	2.80	167
O29...O^{γ}_S263	2.67	159
O27...N^{ζ}_K262	2.75	171
O22...N_K262	2.86	173
IDD594–protein		
O33...O^{H}_Y48	2.73	174
O34...$N^{\varepsilon 1}$_W111	3.07	154
O29...$N^{H\Gamma}$_R268	3.03	162
N25...$N^{\delta 2}$_N272	3.03	173
O_W584...O25	2.68	165
$O^{\delta 2}$_D43...O15	2.68	147
O^{γ}_S159...N12	2.85	140
$O^{\varepsilon 1}$_Q183...N12	2.90	165
$O^{\varepsilon 1}$_Q183...C20	3.04	136
$O^{\varepsilon 2}$_E271...N24	2.94	156
$O^{\delta 1}$_N272...N24	2.86	148

Fig. 1. Ribbon view of the aldose reductase, $NADP^+$, inhibitor complex , and chemical formula of the inhibitor IDD594.

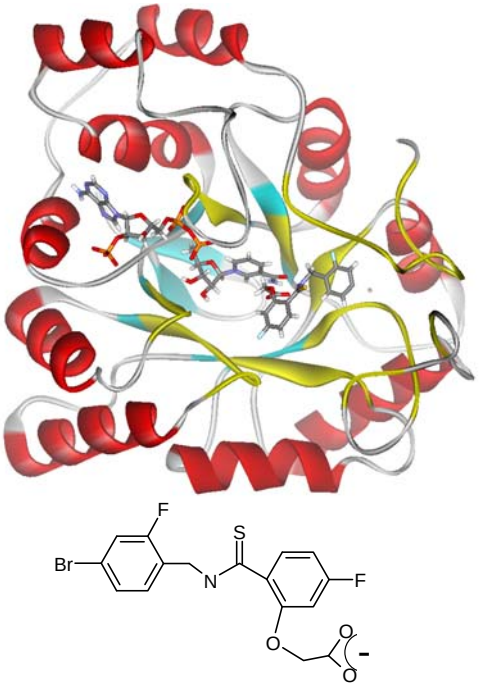

Fig. 2
View of AR structure, with atoms colored according to their temperature factor.
Residues in bold blue describe the structure subset where the charge density was refined.

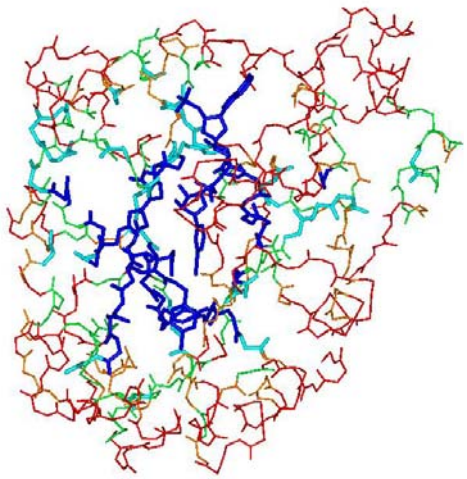

(!!! should be in same orientation as fig 1 !!!)

Fig. 3: Electrostatic potential generated by the $NADP^+$ cofactor in the plane of the nicotinamide ring.
experimental (left), theoretical (right).
Contour levels in all figures are: +/-0.05 e/Å, blue: positive, red: negative, black dotted line: zero level.

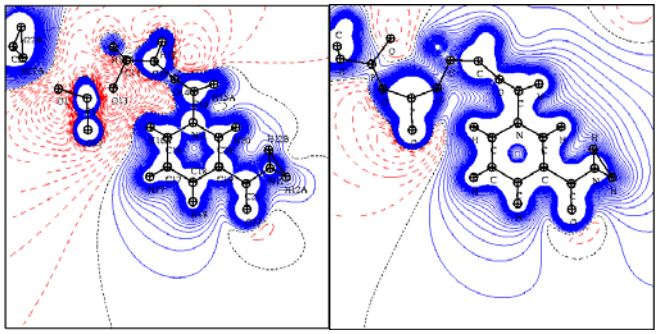

Fig. 4: Active site electrostatic potential in the plane of the nicotinamide ring of the $NADP^+$ cofactor. Theoretical (a), experimental database transferred TRF (b), refined MUL (c), point charges [AMBER] (d).

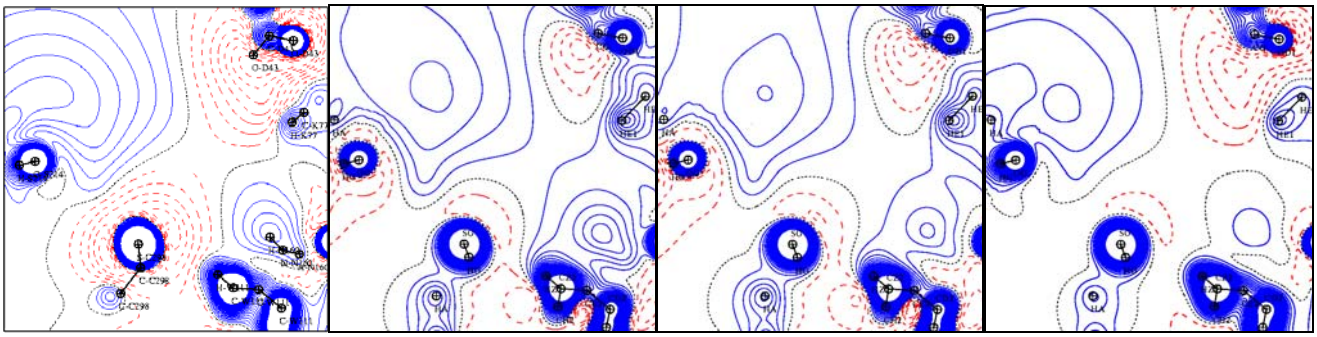

(a) (b) (c) (d)

Fig. 5: (a) Electrostatic potentials of the inhibitor alone. Electrostatic potential of the apoenzyme (in the same plane) (b) theoretical DFT, (c): transferred experimental database TRF, (d) : refined MUL.

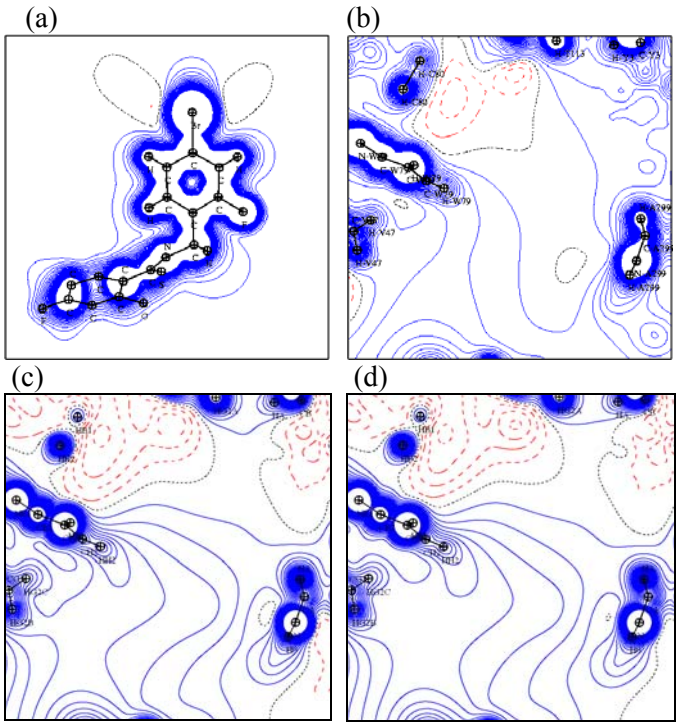

Fig. 6: Theoretical electrostatic potentials for the Br atom in the ligand alone. (a), for the O-T113 in the active site (b), in the aldose reductase complex (c). Transferred experimental potential TRF (d). The plane is the same for all maps.

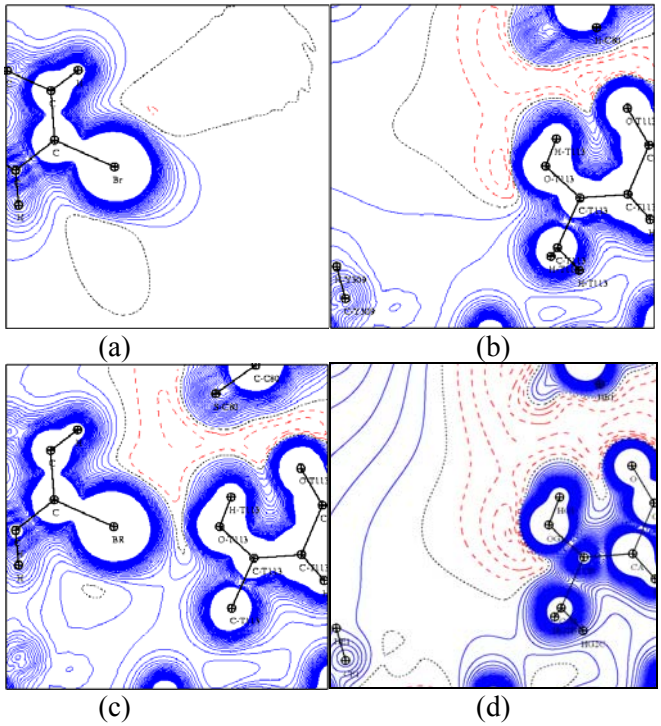

(a) (b)

(c) (d)

Fig. 7: Theoretical Deformation density maps of the Br···OG1-T113 region, in the complex and alone. The map in the left column are in the Br…O-H plane (a). The maps in the middle and right columns display the bromine deformation density of toric shape in the plane perpendicular to the C-Br bond in the complex (b) and for the inhibitor alone (c).

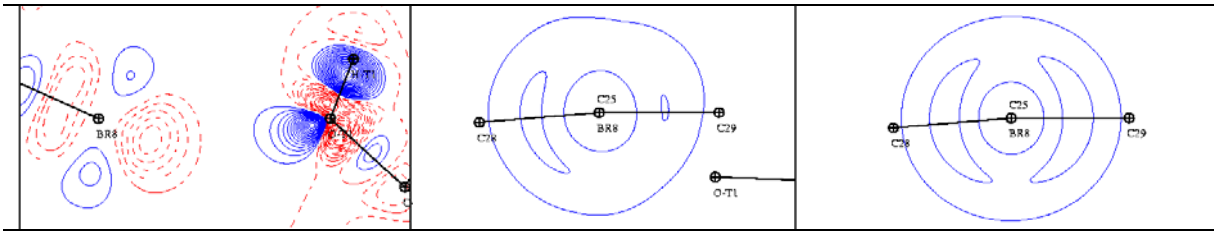

(a) *(b)* *(c)*

Fig. 8: Theoretical electrostatic potential maps (DFT) of the carboxylate region: for the ligand alone (a); for the apoenzyme the active site (b); and for the aldose reductase complex (c). Transferred experimental potential TRF of the active site only (d).

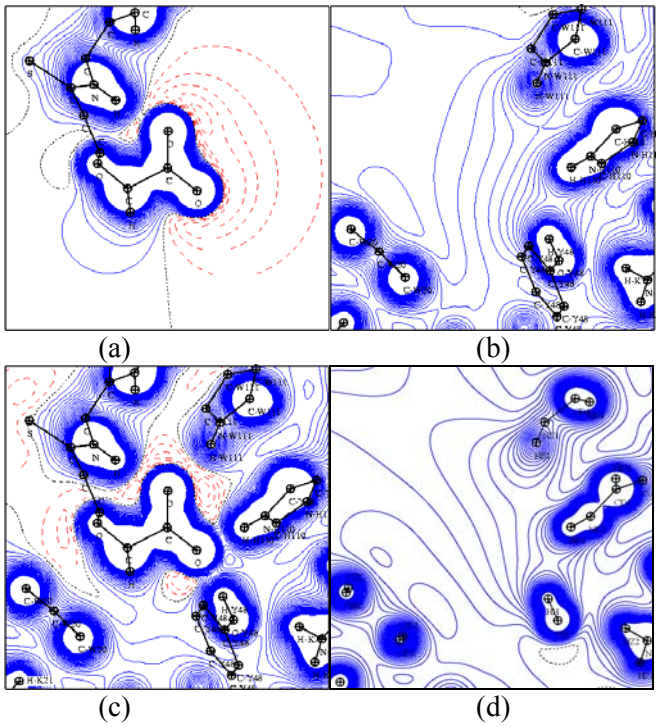

(a) (b)

(c) (d)

Fig. 9: Theoretical electrostatic potentials in the plane perpendicular to the inhibitor carboxylate. (a) protein alone; (b) inhibitor alone; (c) protein + $NADP^+$; (d) transferred experimental database TRF.

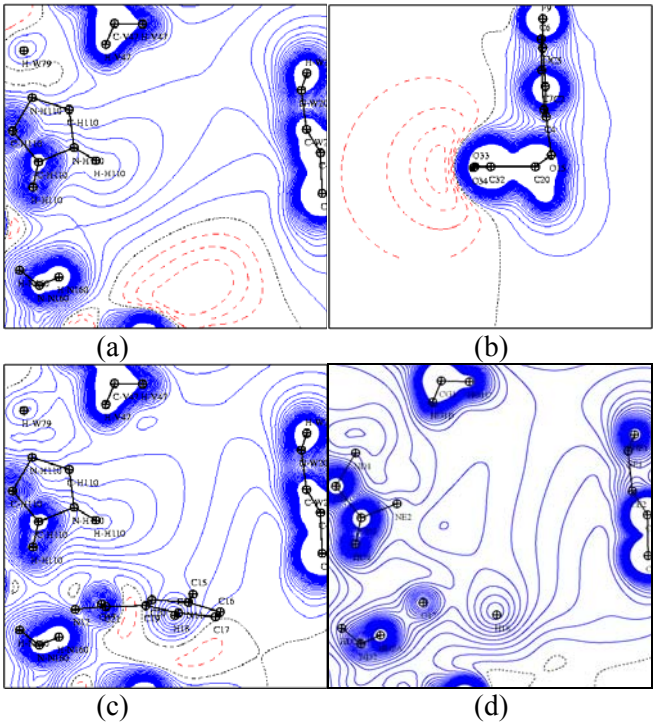

(a) (b)

(c) (d)